

Square-lattice $s = \frac{1}{2}$ XY model and the Jordan–Wigner fermions: The ground–state and thermodynamic properties

Oleg Derzhko^{†,‡}, Taras Verkholyak[†], Reimar Schmidt^{*} and Johannes Richter^{*}

[†]Institute for Condensed Matter Physics,

1 Svientsitskii Street, L’viv–11, 79011, Ukraine

[‡]Chair of Theoretical Physics, Ivan Franko National University of L’viv,

12 Drahomanov Street, L’viv–5, 79005, Ukraine

^{*}Institut für Theoretische Physik, Universität Magdeburg,

P.O. Box 4120, D–39016 Magdeburg, Germany

October 25, 2018

Abstract

Using the 2D Jordan–Wigner transformation we reformulate the square-lattice $s = \frac{1}{2}$ XY (XZ) model in terms of noninteracting spinless fermions and examine the ground–state and thermodynamic properties of this spin system. We consider the model with two types of anisotropy: the spatial anisotropy interpolating between 2D and 1D lattices and the anisotropy of the exchange interaction interpolating between isotropic XY and Ising interactions. We compare the obtained (approximate) results with exact ones (1D limit, square-lattice Ising model) and other approximate ones (linear spin–wave theory and exact diagonalization data for finite lattices of up to $N = 36$ sites supplemented by finite–size scaling). We discuss the ground–state and thermodynamic properties in dependence on the spatial and exchange interaction anisotropies. We pay special attention to the quantum phase transition driven by the exchange interaction anisotropy as well as to the appearance/disappearance of the zero–temperature magnetization in the quasi–1D limit.

PACS numbers: 75.10.–b

Keywords: square–lattice XY model, 2D Jordan–Wigner fermionization, spin–wave theory, exact diagonalization

Postal address:

Dr. Oleg Derzhko (corresponding author)

Institute for Condensed Matter Physics,

1 Svientsitskii Street, L’viv–11, 79011, Ukraine

tel/fax: 380 322 761978

email: derzhko@icmp.lviv.ua

1 Introduction

The $s = \frac{1}{2}$ Heisenberg model on a square lattice is the well-known basic model in the quantum theory of magnetism which became especially attractive after the discovery of high-temperature superconductors [1, 2]. Much more materials which can be viewed as realizations of the 2D $s = \frac{1}{2}$ Heisenberg model are known at present time. Many analytical and numerical studies analyzing thermodynamics, spin correlations and their dynamics for the 2D $s = \frac{1}{2}$ Heisenberg model were performed during the last fifteen years. One of the (approximate) analytical approaches is based on the 2D Jordan–Wigner fermionization. An extension of the 1D Jordan–Wigner transformation for higher dimensions was suggested in the late 80s [3] (see also [4, 5, 6]). Such kind of approximate treatment was applied to the square-lattice quantum spin models in several papers [3, 4, 5, 7] (for a brief review see [8]). Recently, the 2D Jordan–Wigner mapping has been used for the calculation of the magnetization curves of several 2D spin systems [9]. The reported studies [3, 4, 5, 7, 9] deal with the $s = \frac{1}{2}$ isotropic Heisenberg or the $s = \frac{1}{2}$ isotropic XY models and the effects of anisotropic XY exchange interaction were not considered. Another intriguing problem in the theory of magnetism is the influence of the spatial anisotropy on the properties of quantum spin models between the limiting cases of a system of noninteracting chains and of a spatially isotropic 2D system. The issue of disappearing of long-range order in 1D limit although discussed by several authors (see, for example, the papers [10, 11, 12, 13] on the crossover from one to two dimensions for the $s = \frac{1}{2}$ Heisenberg model) remains ambiguous.

In this paper we consider the $s = \frac{1}{2}$ anisotropic XY model on a spatially anisotropic square lattice using the 2D Jordan–Wigner fermionization approach in order 1) to examine the effects of exchange interaction anisotropy and the effects of spatial anisotropy on the ground-state and thermodynamic properties of the spin model and 2) to gain an understanding how well this technique works comparing the approximate results with the exact ones (1D limit, the Onsager solution for the square-lattice Ising model). To examine the quality of the 2D Jordan–Wigner fermionization scheme in the cases for which exact results are not available we perform linear spin-wave theory calculations and finite-size scaling analysis of exact diagonalization data. The 2D Jordan–Wigner fermionization may be used for a study of the dynamic properties of 2D quantum spin systems [14] and a first test of this approach for calculating the static quantities is strongly desirable.

There has been a great deal of theoretical work on the 2D $s = \frac{1}{2}$ XY model [15, 16, 17, 18, 19, 20, 21, 22, 23, 24, 25, 26]. We use the results reported in these papers in our study for comparison in due course. Thus, in Ref. [17] it was shown how the spin-wave theory can be applied to the quantum XY Hamiltonians. Already the very early studies on square-lattice $s = \frac{1}{2}$ isotropic XY model indicated the long-range order in the ground state.

Later the existence of long-range order in the ground state of quantum XY model on a hypercubic lattice in two and higher dimensions was proved rigorously [18]. The exact diagonalization study for the isotropic XY model on finite square lattices of up to 6×6 sites supplemented by finite-size scaling was reported in Ref. [21]. The high precision quantum Monte Carlo results presented in Ref. [22] concern with both the properties at zero and nonzero temperatures. The zero-temperature properties of the square-lattice $s = \frac{1}{2}$ anisotropic XY model were studied via spin-wave theory and via series expansions around the Ising limit [23]. The papers [24, 25] contain the zero-temperature results of the coupled cluster method and the correlated basis function method applied on the square-lattice $s = \frac{1}{2}$ anisotropic XY model, respectively. The Green's-function approach was used for the calculation of the temperature dependences of the susceptibilities and specific heat of the square-lattice $s = \frac{1}{2}$ isotropic XY model in Ref. [26]. It should be remarked that the mentioned studies refer to the spatially isotropic lattices.

This paper is organized as follows. In Section 2 we present the conventional linear spin-wave theory for the square-lattice $s = \frac{1}{2}$ XY model. This consideration is a straightforward generalization of Ref. [17] for the anisotropic case and is given here for easy references. In Section 3 we present the 2D Jordan-Wigner fermionization treatment of the XY and XZ Hamiltonians. The results derived in this Section are parallel to those obtained on the basis of the spin-wave theory and resemble strongly some outcomes of the coupled cluster method and the correlated basis function method [24, 25]. In Section 4 we present the finite-size scaling analysis of the exact diagonalization data. In Section 5 we discuss the effects of anisotropies on the ground-state and thermodynamic properties of the square-lattice $s = \frac{1}{2}$ XY model. We compare the results of different approaches focusing on the validity of the approximate treatment based on the 2D Jordan-Wigner fermionization. Finally, we summarize our findings in Section 6. Some preliminary results of this study were announced in the conference papers [27].

2 The model. Linear spin-wave theory

We consider a model consisting of $N = N_x N_y$ ($N_x = N_y = \sqrt{N} \rightarrow \infty$) spins $\frac{1}{2}$ on a spatially anisotropic square lattice governed by the anisotropic XY Hamiltonian

$$\begin{aligned}
H &= \sum_{i=0}^{N_x-1} \sum_{j=0}^{N_y-1} (J ((1 + \gamma) s_{i,j}^x s_{i+1,j}^x + (1 - \gamma) s_{i,j}^y s_{i+1,j}^y)) \\
&\quad + J_{\perp} ((1 + \gamma) s_{i,j}^x s_{i,j+1}^x + (1 - \gamma) s_{i,j}^y s_{i,j+1}^y)) \\
&= \frac{1}{2} \sum_{i=0}^{N_x-1} \sum_{j=0}^{N_y-1} (J (s_{i,j}^+ s_{i+1,j}^- + s_{i,j}^- s_{i+1,j}^+ + \gamma (s_{i,j}^+ s_{i+1,j}^+ + s_{i,j}^- s_{i+1,j}^-)))
\end{aligned}$$

$$+J_{\perp} (s_{i,j}^+ s_{i,j+1}^- + s_{i,j}^- s_{i,j+1}^+ + \gamma (s_{i,j}^+ s_{i,j+1}^+ + s_{i,j}^- s_{i,j+1}^-)) . \quad (2.1)$$

Here J and J_{\perp} ($= RJ$) are the exchange interaction strengths between neighbouring sites in a row (horizontal direction) and a column (vertical direction), respectively, and the parameter γ controls the anisotropy of exchange interaction. Since the considered lattice is a bipartite one, the cases of ferromagnetic and antiferromagnetic signs of exchange interactions are related to each other by a simple spin rotation. Therefore, in what follows we assume without loss of generality the ferromagnetic sign of the exchange interactions J and J_{\perp} , i.e., $J, J_{\perp} < 0$. We can recover the 1D limit putting either $J_{\perp} = 0$ or $J = 0$ arriving at a system of independent chains running in horizontal or vertical direction, respectively. The case $\gamma = 0$ corresponds to the isotropic XY interaction, whereas the case $\gamma = 1$ (or $\gamma = -1$) corresponds to the Ising interaction. We are interested in the ground-state and thermodynamic properties of spin model (2.1).

We begin with the linear spin-wave theory following the scheme developed in [17]. The conventional spin-wave analysis starts from a ferromagnetic state fully polarized in z direction [28]. We have to deal with the XZ model rather than the XY model. The former Hamiltonian arises from the latter one after the unitary transformation $s^x \rightarrow -s^z$, $s^y \rightarrow s^x$, $s^z \rightarrow -s^y$, and hence exhibits the same thermodynamics. (Evidently, within approximate approaches in which the x, y spin components are treated differently than the z spin components we may expect different results for the XY and XZ models.) The performed rotation is also employed within the coupled cluster method [24] or correlated basis function method [25] applied to the quantum XY model (but not for exact diagonalization computations). Thus, we consider

$$\begin{aligned} H &= \sum_{i=0}^{N_x-1} \sum_{j=0}^{N_y-1} (J ((1-\gamma) s_{i,j}^x s_{i+1,j}^x + (1+\gamma) s_{i,j}^z s_{i+1,j}^z) \\ &\quad + J_{\perp} ((1-\gamma) s_{i,j}^x s_{i,j+1}^x + (1+\gamma) s_{i,j}^z s_{i,j+1}^z)) \\ &= \sum_{i=0}^{N_x-1} \sum_{j=0}^{N_y-1} \left(J \frac{1-\gamma}{4} (s_{i,j}^+ s_{i+1,j}^+ + s_{i,j}^+ s_{i+1,j}^- + s_{i,j}^- s_{i+1,j}^+ + s_{i,j}^- s_{i+1,j}^-) \right. \\ &\quad \left. + J (1+\gamma) \left(s_{i,j}^+ s_{i,j}^- - \frac{1}{2} \right) \left(s_{i+1,j}^+ s_{i+1,j}^- - \frac{1}{2} \right) \right. \\ &\quad \left. + J_{\perp} \frac{1-\gamma}{4} (s_{i,j}^+ s_{i,j+1}^+ + s_{i,j}^+ s_{i,j+1}^- + s_{i,j}^- s_{i,j+1}^+ + s_{i,j}^- s_{i,j+1}^-) \right. \\ &\quad \left. + J_{\perp} (1+\gamma) \left(s_{i,j}^+ s_{i,j}^- - \frac{1}{2} \right) \left(s_{i,j+1}^+ s_{i,j+1}^- - \frac{1}{2} \right) \right) . \quad (2.2) \end{aligned}$$

Employing the Holstein-Primakoff transformation we arrive at the following Hamiltonian of the linear spin-wave theory

$$H = \sum_{i=0}^{N_x-1} \sum_{j=0}^{N_y-1} \left(J \frac{1-\gamma}{4} (a_{i,j}^+ a_{i+1,j}^+ + a_{i,j}^+ a_{i+1,j}^- + a_{i,j}^- a_{i+1,j}^+ + a_{i,j}^- a_{i+1,j}^-) \right.$$

$$\begin{aligned}
& +J(1+\gamma) \left(\frac{1}{4} - \frac{1}{2} a_{i,j}^+ a_{i,j} - \frac{1}{2} a_{i+1,j}^+ a_{i+1,j} \right) \\
& +J_{\perp} \frac{1-\gamma}{4} \left(a_{i,j}^+ a_{i,j+1}^+ + a_{i,j}^+ a_{i,j+1} + a_{i,j} a_{i,j+1}^+ + a_{i,j} a_{i,j+1} \right) \\
& +J_{\perp}(1+\gamma) \left(\frac{1}{4} - \frac{1}{2} a_{i,j}^+ a_{i,j} - \frac{1}{2} a_{i,j+1}^+ a_{i,j+1} \right), \tag{2.3}
\end{aligned}$$

where the operators $a_{i,j}^+$, $a_{i,j}$ obey the Bose commutation rules. After performing the Fourier transformation

$$a_{i,j} = \frac{1}{\sqrt{N_x N_y}} \sum_{k_x, k_y} e^{i(k_x i + k_y j)} a_{k_x, k_y}, \quad a_{i,j}^+ = \frac{1}{\sqrt{N_x N_y}} \sum_{k_x, k_y} e^{-i(k_x i + k_y j)} a_{k_x, k_y}^+ \tag{2.4}$$

with $k_x = \frac{2\pi}{N_x} n_x$, $n_x = -\frac{N_x}{2}, -\frac{N_x}{2} + 1, \dots, \frac{N_x}{2} - 1$, $k_y = \frac{2\pi}{N_y} n_y$, $n_y = -\frac{N_y}{2}, -\frac{N_y}{2} + 1, \dots, \frac{N_y}{2} - 1$ (N_x, N_y are even) we come to the following quadratic form

$$\begin{aligned}
H = \frac{1}{4} \sum_{\mathbf{k}} & \left((1-\gamma) J_{\mathbf{k}} - 2(1+\gamma)(J+J_{\perp}) \right) (a_{\mathbf{k}}^+ a_{\mathbf{k}} + a_{-\mathbf{k}} a_{-\mathbf{k}}^+) + (1-\gamma) J_{\mathbf{k}} (a_{\mathbf{k}}^+ a_{-\mathbf{k}}^+ + a_{\mathbf{k}} a_{-\mathbf{k}}) \\
& + \frac{3}{4} N(1+\gamma)(J+J_{\perp}), \tag{2.5} \\
& J_{\mathbf{k}} = J \cos k_x + J_{\perp} \cos k_y.
\end{aligned}$$

This quadratic form (2.5) can be diagonalized by the Bogolyubov transformation

$$\begin{aligned}
a_{\mathbf{k}} &= (\cosh u_{\mathbf{k}}) b_{\mathbf{k}} + (\sinh u_{\mathbf{k}}) b_{-\mathbf{k}}^+, \\
a_{-\mathbf{k}}^+ &= (\sinh u_{\mathbf{k}}) b_{\mathbf{k}} + (\cosh u_{\mathbf{k}}) b_{-\mathbf{k}}^+, \tag{2.6}
\end{aligned}$$

where the real function $u_{\mathbf{k}} = u_{-\mathbf{k}}$ is given by the equation

$$\tanh(2u_{\mathbf{k}}) = \frac{(1-\gamma) J_{\mathbf{k}}}{2(1+\gamma)(J+J_{\perp}) - (1-\gamma) J_{\mathbf{k}}}. \tag{2.7}$$

As a result we get

$$\begin{aligned}
H &= \sum_{\mathbf{k}} \Omega_{\mathbf{k}} \left(b_{\mathbf{k}}^+ b_{\mathbf{k}} + \frac{1}{2} \right) + \frac{3}{4} N(1+\gamma)(J+J_{\perp}), \tag{2.8} \\
\Omega_{\mathbf{k}} &= \sqrt{(1+\gamma)^2 (J+J_{\perp})^2 - (1-\gamma)^2 (J+J_{\perp}) J_{\mathbf{k}}}.
\end{aligned}$$

In the special case $\gamma = 0$, $J = J_{\perp}$ Eq. (2.8) reproduces the result derived in Ref. [17].

Now we can calculate in the usual way the ground-state energy per site

$$e_0 = \frac{1}{2} \int_{-\pi}^{\pi} \frac{dk_x}{2\pi} \int_{-\pi}^{\pi} \frac{dk_y}{2\pi} \Omega_{\mathbf{k}} + \frac{3}{4} (1+\gamma)(J+J_{\perp}) \tag{2.9}$$

and the zero-temperature (z) magnetization per site

$$m^z = -\frac{1}{2} \int \frac{d\mathbf{k}}{(2\pi)^2} \frac{1}{\sqrt{1 - \tanh^2(2u_{\mathbf{k}})}} + 1 \tag{2.10}$$

(keeping in mind that $s^z = \frac{1}{2} - a^+ a$).

Let us note that the approximate treatment which starts from Eq. (2.3) has destroyed the symmetry with respect to the change γ to $-\gamma$. Moreover, the consideration is valid only for $\gamma \geq 0$ otherwise there exist such values of \mathbf{k} at which the r.h.s. of (2.7) for $\tanh(2u_{\mathbf{k}})$ exceeds 1. Evidently, while getting (2.3) we have presumed the long-range order in z direction in the spin space and this assumption becomes wrong if $\gamma < 0$.

3 2D Jordan–Wigner fermions: XY vs. XZ

An alternative approach to calculate the thermodynamic quantities of the square-lattice $s = \frac{1}{2}$ XY model consists in the 2D Jordan–Wigner transformation reformulating the problem in fermionic language. First we introduce the annihilation and creation operators of spinless fermions

$$\begin{aligned} s_{i,j}^- &= e^{i\alpha_{i,j}} d_{i,j}, & s_{i,j}^+ &= e^{-i\alpha_{i,j}} d_{i,j}^+, \\ \alpha_{i,j} &= \sum_{f(\neq i)} \sum_{g(\neq j)} \text{Im} \ln(f - i + i(g - j)) d_{f,g}^+ d_{f,g} \end{aligned} \quad (3.1)$$

transforming (2.1) into

$$\begin{aligned} H &= \frac{1}{2} \sum_{i=0}^{N_x-1} \sum_{j=0}^{N_y-1} \left(J \left(d_{i,j}^+ e^{i(\alpha_{i+1,j} - \alpha_{i,j})} d_{i+1,j} + d_{i,j} e^{-i(\alpha_{i+1,j} - \alpha_{i,j})} d_{i+1,j}^+ \right. \right. \\ &\quad \left. \left. + \gamma \left(d_{i,j}^+ e^{-i(\alpha_{i+1,j} + \alpha_{i,j})} d_{i+1,j}^+ + d_{i,j} e^{i(\alpha_{i+1,j} + \alpha_{i,j})} d_{i+1,j} \right) \right) \right. \\ &\quad \left. + J_{\perp} \left(d_{i,j}^+ e^{i(\alpha_{i,j+1} - \alpha_{i,j})} d_{i,j+1} + d_{i,j} e^{-i(\alpha_{i,j+1} - \alpha_{i,j})} d_{i,j+1}^+ \right. \right. \\ &\quad \left. \left. + \gamma \left(d_{i,j}^+ e^{-i(\alpha_{i,j+1} + \alpha_{i,j})} d_{i,j+1}^+ + d_{i,j} e^{i(\alpha_{i,j+1} + \alpha_{i,j})} d_{i,j+1} \right) \right) \right). \end{aligned} \quad (3.2)$$

We adopt a mean-field treatment of the phase factors which have appeared in the Hamiltonian (3.2) replacing the fermion occupation-number operators by their average value $\frac{1}{2}$ and using the same gauge as in Ref. [4] (see also Refs. [3, 8]). As a result we arrive at

$$\begin{aligned} H &= \frac{1}{2} \sum_{i=0}^{N_x-1} \sum_{j=0}^{N_y-1} \left(J (-1)^{i+j} \left(d_{i,j}^+ d_{i+1,j} - d_{i,j} d_{i+1,j}^+ + \gamma \left(d_{i,j}^+ d_{i+1,j}^+ - d_{i,j} d_{i+1,j} \right) \right) \right. \\ &\quad \left. + J_{\perp} \left(d_{i,j}^+ d_{i,j+1} - d_{i,j} d_{i,j+1}^+ + \gamma \left(d_{i,j}^+ d_{i,j+1}^+ - d_{i,j} d_{i,j+1} \right) \right) \right). \end{aligned} \quad (3.3)$$

This is the only approximate step made to derive the thermodynamic quantities of the spin model (2.1) within the 2D Jordan–Wigner fermionization approach. Further consideration requires no approximations. Next we perform the Fourier transformation

$$d_{i,j} = \frac{1}{\sqrt{N_x N_y}} \sum_{k_x, k_y} e^{i(k_x i + k_y j)} d_{k_x, k_y}, \quad d_{i,j}^+ = \frac{1}{\sqrt{N_x N_y}} \sum_{k_x, k_y} e^{-i(k_x i + k_y j)} d_{k_x, k_y}^+ \quad (3.4)$$

with $k_x = \frac{2\pi}{N_x}n_x$, $n_x = -\frac{N_x}{2}, -\frac{N_x}{2} + 1, \dots, \frac{N_x}{2} - 1$, $k_y = \frac{2\pi}{N_y}n_y$, $n_y = -\frac{N_y}{2}, -\frac{N_y}{2} + 1, \dots, \frac{N_y}{2} - 1$ (N_x, N_y are even).

As a result Eq. (3.3) becomes

$$H = \frac{1}{2} \sum_{\mathbf{k}}' \begin{pmatrix} d_{k_x, k_y}^+ & d_{-k_x, -k_y} & d_{k_x \pm \pi, k_y \pm \pi}^+ & d_{-k_x \pm \pi, -k_y \pm \pi} \end{pmatrix} \\ \times \begin{pmatrix} A & iB & -iC & -D \\ -iB & -A & D & iC \\ iC & D & -A & -iB \\ -D & -iC & iB & A \end{pmatrix} \begin{pmatrix} d_{k_x, k_y} \\ d_{-k_x, -k_y}^+ \\ d_{k_x \pm \pi, k_y \pm \pi} \\ d_{-k_x \pm \pi, -k_y \pm \pi}^+ \end{pmatrix}, \\ A = J_{\perp} \cos k_y, \quad B = \gamma J_{\perp} \sin k_y, \quad C = J \sin k_x, \quad D = \gamma J \cos k_x. \quad (3.5)$$

Here the prime denotes that \mathbf{k} in the thermodynamic limit varies in the region $-\pi \leq k_y \leq \pi$, $-\pi + |k_y| \leq k_x \leq \pi - |k_y|$. The 4×4 matrix in (3.5) can be diagonalized. Its eigenvalues $\Lambda_{\alpha}(\mathbf{k})$ are given by

$$\Lambda_1(\mathbf{k}) = \sqrt{(J_{\perp} \cos k_y + \gamma J \cos k_x)^2 + (J \sin k_x + \gamma J_{\perp} \sin k_y)^2}, \\ \Lambda_2(\mathbf{k}) = \sqrt{(J_{\perp} \cos k_y - \gamma J \cos k_x)^2 + (J \sin k_x - \gamma J_{\perp} \sin k_y)^2}, \\ \Lambda_3(\mathbf{k}) = -\Lambda_1(\mathbf{k}), \\ \Lambda_4(\mathbf{k}) = -\Lambda_2(\mathbf{k}). \quad (3.6)$$

Therefore, the Hamiltonian (3.5) then assumes the form

$$H = \sum_{\mathbf{k}}' \sum_{\alpha=1}^2 \Lambda_{\alpha}(\mathbf{k}) \left(\eta_{\mathbf{k}, \alpha}^+ \eta_{\mathbf{k}, \alpha} - \frac{1}{2} \right), \quad (3.7)$$

where $\eta_{\mathbf{k}, \alpha}, \eta_{\mathbf{k}, \alpha}^+$, $\alpha = 1, 2$ are Fermi operators.

It is easy to calculate now the Helmholtz free energy per site

$$f = -\frac{1}{2\beta} \int_{-\pi}^{\pi} \frac{dk_x}{2\pi} \int_{-\pi}^{\pi} \frac{dk_y}{2\pi} \left(\ln \left(2 \cosh \frac{\beta \Lambda_1(\mathbf{k})}{2} \right) + \ln \left(2 \cosh \frac{\beta \Lambda_2(\mathbf{k})}{2} \right) \right). \quad (3.8)$$

The ground-state energy per site which follows from (3.8) in the zero-temperature limit $\beta \rightarrow \infty$ reads

$$e_0 = -\frac{1}{4} \int \frac{d\mathbf{k}}{(2\pi)^2} (\Lambda_1(\mathbf{k}) + \Lambda_2(\mathbf{k})). \quad (3.9)$$

The entropy and specific heat according to Eq. (3.8) are as follows

$$\frac{s}{k} = \frac{1}{2} \int \frac{d\mathbf{k}}{(2\pi)^2} \left(\ln \left(2 \cosh \frac{\beta \Lambda_1(\mathbf{k})}{2} \right) + \ln \left(2 \cosh \frac{\beta \Lambda_2(\mathbf{k})}{2} \right) \right) \\ - \frac{1}{2} \int \frac{d\mathbf{k}}{(2\pi)^2} \left(\frac{\beta \Lambda_1(\mathbf{k})}{2} \tanh \frac{\beta \Lambda_1(\mathbf{k})}{2} + \frac{\beta \Lambda_2(\mathbf{k})}{2} \tanh \frac{\beta \Lambda_2(\mathbf{k})}{2} \right), \quad (3.10)$$

$$\frac{c}{k} = \frac{1}{2} \int \frac{d\mathbf{k}}{(2\pi)^2} \left(\left(\frac{\frac{\beta\Lambda_1(\mathbf{k})}{2}}{\cosh \frac{\beta\Lambda_1(\mathbf{k})}{2}} \right)^2 + \left(\frac{\frac{\beta\Lambda_2(\mathbf{k})}{2}}{\cosh \frac{\beta\Lambda_2(\mathbf{k})}{2}} \right)^2 \right). \quad (3.11)$$

In 1D limit formulas (3.6), (3.8) – (3.11) yield the long-known exact results for the thermodynamic quantities of spin- $\frac{1}{2}$ anisotropic XY chain. Note, that the symmetry with respect to the change γ to $-\gamma$ inherent in the original spin model is present in the fermionic description (3.7), (3.6).

We cannot calculate the magnetization m^x (or m^y) by averaging $s_{i,j}^x$ (or $s_{i,j}^y$) because of the invariance of the Hamiltonian (2.1) when all $s_{i,j}^x \rightarrow -s_{i,j}^x$ (or all $s_{i,j}^y \rightarrow -s_{i,j}^y$); this symmetry remains in the approximate treatment as well. m^x (or m^y) can be obtained as a square root of the two-site correlation function of x (or y) spin components taken at sites which are at infinitely large distance. However, to our best knowledge such correlation functions have not been examined within the 2D Jordan–Wigner fermionization approach up till now.

In the second part of this Section we consider the XZ rather than the XY Hamiltonian. We start from the Hamiltonian (2.2). Making use of the transformation (3.1) and adopting the mean-field treatment of phase factors as used already for obtaining (3.3) we get the following Hamiltonian of interacting spinless fermions on a square lattice

$$\begin{aligned} H = \sum_{i=0}^{N_x-1} \sum_{j=0}^{N_y-1} & \left(J(-1)^{i+j} \frac{1-\gamma}{4} (d_{i,j}^+ d_{i+1,j}^+ + d_{i,j}^+ d_{i+1,j} - d_{i,j} d_{i+1,j}^+ - d_{i,j} d_{i+1,j}) \right. \\ & + J(1+\gamma) \left(d_{i,j}^+ d_{i,j} - \frac{1}{2} \right) \left(d_{i+1,j}^+ d_{i+1,j} - \frac{1}{2} \right) \\ & + J_{\perp} \frac{1-\gamma}{4} (d_{i,j}^+ d_{i,j+1}^+ + d_{i,j}^+ d_{i,j+1} - d_{i,j} d_{i,j+1}^+ - d_{i,j} d_{i,j+1}) \\ & \left. + J_{\perp} (1+\gamma) \left(d_{i,j}^+ d_{i,j} - \frac{1}{2} \right) \left(d_{i,j+1}^+ d_{i,j+1} - \frac{1}{2} \right) \right). \end{aligned} \quad (3.12)$$

We need further approximations because of the interaction terms in Eq. (3.12). We may assume that

$$\begin{aligned} d_{i,j}^+ d_{i,j} d_{i+1,j}^+ d_{i+1,j} & \rightarrow m d_{i,j}^+ d_{i,j} + \frac{1}{2} d_{i,j}^+ d_{i,j} + m d_{i+1,j}^+ d_{i+1,j} + \frac{1}{2} d_{i+1,j}^+ d_{i+1,j} - \frac{1}{4} - m^2 - m, \\ d_{i,j}^+ d_{i,j} d_{i,j+1}^+ d_{i,j+1} & \rightarrow m d_{i,j}^+ d_{i,j} + \frac{1}{2} d_{i,j}^+ d_{i,j} + m d_{i,j+1}^+ d_{i,j+1} + \frac{1}{2} d_{i,j+1}^+ d_{i,j+1} - \frac{1}{4} - m^2 - m, \end{aligned} \quad (3.13)$$

i.e., (ferromagnetic) long-range order (the existence of which in two dimensions is proved rigorously for $\gamma = 0$ at zero temperature or for $\gamma = 1$ at nonzero temperature) is imposed. The order parameter is $m = m^z$ and its nonzero value may be expected for positive γ . For negative γ one may apply the unitary transformation $s^x \rightarrow s^z$, $s^y \rightarrow s^y$, $s^z \rightarrow -s^x$ coming back to the model with positive γ . Thus the thermodynamics of the model with positive γ and $m = m^z$ is the same as of the model with negative γ and $m = m^x$. These symmetry arguments permit us to find the thermodynamic properties of the model (2.2) also for $\gamma \leq 0$ basing on the results calculated for $\gamma \geq 0$.

Performing further the Fourier transformation (3.4) one gets

$$H = \frac{1}{2} \sum_{\mathbf{k}}' \begin{pmatrix} d_{k_x, k_y}^+ & d_{-k_x, -k_y} & d_{k_x \pm \pi, k_y \pm \pi}^+ & d_{-k_x \pm \pi, -k_y \pm \pi} \end{pmatrix} \times \begin{pmatrix} \mathcal{A} + \mathcal{M} & i\mathcal{B} & -i\mathcal{C} & -\mathcal{D} \\ -i\mathcal{B} & -\mathcal{A} - \mathcal{M} & \mathcal{D} & i\mathcal{C} \\ i\mathcal{C} & \mathcal{D} & -\mathcal{A} + \mathcal{M} & -i\mathcal{B} \\ -\mathcal{D} & -i\mathcal{C} & i\mathcal{B} & \mathcal{A} - \mathcal{M} \end{pmatrix} \begin{pmatrix} d_{k_x, k_y} \\ d_{-k_x, -k_y}^+ \\ d_{k_x \pm \pi, k_y \pm \pi} \\ d_{-k_x \pm \pi, -k_y \pm \pi}^+ \end{pmatrix} - N(1 + \gamma)(J + J_{\perp})m^2 \quad (3.14)$$

with

$$\mathcal{A} = \frac{1 - \gamma}{2} J_{\perp} \cos k_y, \quad \mathcal{B} = \frac{1 - \gamma}{2} J_{\perp} \sin k_y, \quad \mathcal{C} = \frac{1 - \gamma}{2} J \sin k_x, \quad \mathcal{D} = \frac{1 - \gamma}{2} J \cos k_x, \quad \mathcal{M} = 2(1 + \gamma)(J + J_{\perp})m. \quad (3.15)$$

The 4×4 matrix in (3.14) can be diagonalized. Its eigenvalues $\Lambda_{\alpha}(\mathbf{k})$ are given by

$$\Lambda_{1,2}(\mathbf{k}) = \sqrt{\mathcal{A}^2 + \mathcal{B}^2 + \mathcal{C}^2 + \mathcal{D}^2 + \mathcal{M}^2 \pm 2\sqrt{(\mathcal{A}\mathcal{D} + \mathcal{B}\mathcal{C})^2 + (\mathcal{A}^2 + \mathcal{C}^2)\mathcal{M}^2}}, \quad \Lambda_{3,4}(\mathbf{k}) = -\Lambda_{1,2}(\mathbf{k}). \quad (3.16)$$

Therefore, the resulting fermionic Hamiltonian assumes the form

$$H = \sum_{\mathbf{k}}' \sum_{\alpha=1}^2 \Lambda_{\alpha}(\mathbf{k}) \left(\eta_{\mathbf{k},\alpha}^+ \eta_{\mathbf{k},\alpha} - \frac{1}{2} \right) - N(1 + \gamma)(J + J_{\perp})m^2 \quad (3.17)$$

with $\Lambda_{\alpha}(\mathbf{k})$ (3.16).

The Helmholtz free energy per site is given by

$$f = -\frac{1}{2\beta} \int \frac{d\mathbf{k}}{(2\pi)^2} \left(\ln \left(2 \cosh \frac{\beta\Lambda_1(\mathbf{k})}{2} \right) + \ln \left(2 \cosh \frac{\beta\Lambda_2(\mathbf{k})}{2} \right) \right) + (1 + \gamma)(|J| + |J_{\perp}|)m^2 \quad (3.18)$$

and the magnetization m is determined by minimizing (3.18), i.e., from the following equation

$$2(1 + \gamma)(|J| + |J_{\perp}|)m = \frac{1}{4} \int \frac{d\mathbf{k}}{(2\pi)^2} \left(\frac{\partial\Lambda_1(\mathbf{k})}{\partial m} \tanh \frac{\beta\Lambda_1(\mathbf{k})}{2} + \frac{\partial\Lambda_2(\mathbf{k})}{\partial m} \tanh \frac{\beta\Lambda_2(\mathbf{k})}{2} \right). \quad (3.19)$$

As can be seen from (3.18), (3.19), (3.16), (3.15) the symmetry with respect to the change γ to $-\gamma$ inherent in the spin model (2.2) is destroyed in the elaborated formulas. Evidently, the derived results for the XZ Hamiltonian in the limit $\gamma = -1$ coincide with the results for the XY Hamiltonian with $\gamma = \pm 1$ presented in the first part of this Section.

It can be easily observed that in the limit $\gamma = 1$ the described 2D Jordan–Wigner fermionization approach for the square–lattice $s = \frac{1}{2}$ XZ model yields the mean–field theory of the square–lattice Ising model. Really, Eq.

(3.12) for $\gamma = 1$ (in this case the fermionic representation (3.12) becomes exact since the Ising interaction of z spin components does not involve the phase factors) after decoupling (3.13) becomes

$$\begin{aligned}
H &= \sum_{i=0}^{N_x-1} \sum_{j=0}^{N_y-1} \left(2J \left(d_{i,j}^+ d_{i,j} - \frac{1}{2} \right) \left(d_{i+1,j}^+ d_{i+1,j} - \frac{1}{2} \right) + 2J_{\perp} \left(d_{i,j}^+ d_{i,j} - \frac{1}{2} \right) \left(d_{i,j+1}^+ d_{i,j+1} - \frac{1}{2} \right) \right) \\
&= \sum_{i=0}^{N_x-1} \sum_{j=0}^{N_y-1} (2J (ms_{i,j}^z + ms_{i+1,j}^z - m^2) + 2J_{\perp} (ms_{i,j}^z + ms_{i,j+1}^z - m^2)) \quad (3.20)
\end{aligned}$$

(we have used the relation $s^z = d^+ d - \frac{1}{2}$). Obviously, the Helmholtz free energy per site for the mean-field spin Hamiltonian (3.20) follows also from (3.18) after inserting $\gamma = 1$, i.e., $f = -\frac{1}{\beta} \ln(2 \cosh(2\beta(|J| + |J_{\perp}|)m)) + 2(|J| + |J_{\perp}|)m^2$. The equation for m (3.19) becomes simple

$$m = \frac{1}{2} \tanh(2\beta(|J| + |J_{\perp}|)m) \quad (3.21)$$

and hence we arrive at familiar formulas for the internal energy per site $e = -2(|J| + |J_{\perp}|)m^2$ and the specific heat $\frac{c}{k} = 4\beta^2(|J| + |J_{\perp}|)m \frac{\partial m}{\partial \beta}$.

To close this Section let us note, that a more sophisticated treatment (i.e., a more complicated decoupling of the l.h.s. of (3.13)) of the Hamiltonian (3.12) is possible (see Ref. [8] for a review of analogous studies for the isotropic Heisenberg model). However, we found that this more complicated approximation seems to be less adequate to describe the properties of the spin system.

4 Finite-size scaling analysis of the exact diagonalization data

In this Section we present the results of the exact diagonalization computations of the ground-state energy and the ground-state magnetization for the $s = \frac{1}{2}$ isotropic (i.e., $\gamma = 0$) XY model on small spatially anisotropic (i.e., $0 \leq R \leq 1$) lattices with periodic boundary conditions. The results for e_0 and $m^{x^2} = \frac{1}{N_x^2 N_y^2} \sum_{i_1, i_2=1}^{N_x} \sum_{j_1, j_2=1}^{N_y} \langle s_{i_1, j_1}^x s_{i_2, j_2}^x \rangle$ for spatially anisotropic finite square lattices of $N = N_x N_y$ sites ($N_x = N_y = \sqrt{N} = L$) for $L = 4$ and $L = 6$ of square shape are reported in Table 1. We also calculate e_0 and $m^{x^2} = \frac{1}{N^2} \sum_{m_1=1}^N \sum_{m_2=1}^N \langle s_{m_1}^x s_{m_2}^x \rangle$ for spatially anisotropic finite square lattices of $N = 8, 18, 32$ sites of diamond shape (Table 2). It is worth to remark that according to the adopted definition of m^{x^2} both the results for the square and diamond shaped finite square lattices for $R = 0$ yield the adequate value for a chain divided by the number of isolated chains into which the finite square lattice splits for $R = 0$ (compare, for example, the results from Table 1 and Table 2 for $m^{x^2}(L = 4)$ (4 chains at $R = 0$) and $m^{x^2}(N = 8)$ (2 chains at $R = 0$) or for $m^{x^2}(L = 6)$ (6 chains at $R = 0$) and $m^{x^2}(N = 18)$ (3 chains at $R = 0$)).

Table 1: Exact diagonalization data for the spatially anisotropic $s = \frac{1}{2}$ XY model ($\gamma = 0$) on finite square lattices of square shape.

R	$e_0(L = 4)$	$e_0(L = 6)$	$m^{x^2}(L = 4)$	$m^{x^2}(L = 6)$
0.00	-0.353553	-0.333333	0.045535	0.025463
0.01	-0.353586	-0.333385	0.047178	0.027241
0.02	-0.353684	-0.333541	0.048908	0.029217
0.03	-0.353848	-0.333801	0.050731	0.031427
0.04	-0.354078	-0.334164	0.052652	0.033911
0.05	-0.354375	-0.334632	0.054673	0.036713
0.10	-0.356909	-0.338570	0.066284	0.056225
0.15	-0.361291	-0.345166	0.079674	0.078399
0.20	-0.367541	-0.353772	0.092803	0.092460
0.30	-0.384698	-0.374145	0.111863	0.105124
0.40	-0.405918	-0.396792	0.121758	0.110963
0.50	-0.429449	-0.420846	0.126876	0.114331
0.60	-0.454432	-0.445916	0.129709	0.116406
0.70	-0.480432	-0.471769	0.131334	0.117683
0.80	-0.507203	-0.498253	0.132243	0.118429
0.90	-0.534590	-0.525255	0.132689	0.118804
1.00	-0.562486	-0.552694	0.132816	0.118911

Table 2: Exact diagonalization data for the spatially anisotropic $s = \frac{1}{2}$ XY model ($\gamma = 0$) on finite square lattices of diamond shape.

R	$e_0(N = 8)$	$e_0(N = 18)$	$e_0(N = 32)$	$m^{x^2}(N = 8)$	$m^{x^2}(N = 18)$	$m^{x^2}(N = 32)$
0.00	-0.353553	-0.333333	-0.326641	0.091069	0.050926	0.033695
0.01	-0.353617	-0.333387	-0.326712	0.094262	0.054471	0.037441
0.02	-0.353809	-0.333555	-0.326929	0.097420	0.058335	0.041851
0.03	-0.354127	-0.333845	-0.327298	0.100523	0.062478	0.046982
0.04	-0.354570	-0.334266	-0.327828	0.103553	0.066833	0.052763
0.05	-0.355134	-0.334823	-0.328526	0.106492	0.071311	0.058967
0.10	-0.359648	-0.339627	-0.334342	0.119459	0.092111	0.085177
0.15	-0.366554	-0.347155	-0.342674	0.129211	0.105816	0.097591
0.20	-0.375259	-0.356377	-0.352257	0.136131	0.113676	0.103995
0.30	-0.396250	-0.377584	-0.373529	0.144342	0.121607	0.111009
0.40	-0.420165	-0.400902	-0.396613	0.148511	0.125525	0.114920
0.50	-0.445817	-0.425543	-0.420942	0.150783	0.127801	0.117335
0.60	-0.472609	-0.451135	-0.446204	0.152087	0.129200	0.118862
0.70	-0.500218	-0.477457	-0.472195	0.152846	0.130060	0.119815
0.80	-0.528446	-0.504366	-0.498777	0.153274	0.130561	0.120375
0.90	-0.557169	-0.531756	-0.525847	0.153484	0.130813	0.120657
1.00	-0.586302	-0.559552	-0.553329	0.153543	0.130885	0.120738

From [29, 21, 22] we know that the ground-state energy per site for the case $R = 1$, $\gamma = 0$ scales as

$$e_0(L) = e_0(\infty) + \frac{\epsilon_3}{L^3} + \frac{\epsilon_5}{L^5} + \dots \quad (4.1)$$

From Ref. [30] we know that the finite-size corrections to the ground-state energy per site for the case $R = 0$, $\gamma = 0$ (for both periodic and antiperiodic boundary conditions) scales as

$$e_0(N_x) - e_0(\infty) \sim \frac{1}{N_x^2}. \quad (4.2)$$

To extrapolate the exact diagonalization data with periodic boundary conditions for $0 \leq R \leq 1$ we use the scaling law

$$e_0(L) = e_0(\infty) + \frac{\epsilon}{L^{2+R}} \quad (4.3)$$

which contains two unknown parameters $e_0(\infty)$ and ϵ and yields correct asymptotics in 1D and 2D limits. The same scaling law was used in [12] to extrapolate the exact diagonalization data for spatially anisotropic 2D $s = \frac{1}{2}$ Heisenberg model. Another scaling law which also yields correct asymptotics in 1D and 2D limits and therefore may be assumed to extrapolate the exact diagonalization data for $0 \leq R \leq 1$,

$$e_0(L) = e_0(\infty) + \frac{\epsilon_2}{L^2} + \frac{\epsilon_3}{L^3} + \dots, \quad (4.4)$$

contains three parameters $e_0(\infty)$, ϵ_2 , ϵ_3 to be determined from the exact diagonalization data. Bearing in mind the 2D-to-1D crossover we should note, that the available data for $N = 16, 36$ square lattices cannot be completed by data for $N = 25$ square lattice since the latter lattice for $R \rightarrow 0$ transforms into chains of odd number of sites and the data essentially differ from those for chains of even numbers of sites. The exact diagonalization data for $N = 64$ are far beyond the available computer resources. On the other hand, the lattices of $N = 8, 18, 32$ sites in the limit $R \rightarrow 0$ split into 2, 3, 4 chains of 4, 6, 8 sites and the shape effects become more pronounced.

The simplest assumption for extrapolation of the exact diagonalization data for $m^{x^2}(L)$ for $R = 1$, $\gamma = 0$ (see, for example, [22, 31]) is as follows

$$m^{x^2}(L) = m^{x^2}(\infty) + \frac{\mu_1}{L} + \dots \quad (4.5)$$

We use the finite-size scaling (4.5) to extrapolate the numerical data for $N = 16, 36$ and for $N = 8, 18, 32$ lattices for $0 \leq R \leq 1$. The finite-size scaling analysis of the available data yields incorrect prediction $m^{x^2}(\infty) < 0$ in quasi-1D limit starting from R in between 0.03 and 0.05 (see Section 5 below) that may serve as indication of a disappearance of the long-range order in 1D limit.

From [32] we know that in the 1D case $R = 0$, $\gamma = 0$ x (or y) magnetization vanishes as

$$m^{x^2}(N_x) \sim \frac{1}{\sqrt{N_x}}. \quad (4.6)$$

To obtain $m^{x^2}(\infty)$ for $0 \leq R \leq 1$ we may combine (4.6) and (4.5) and assume $m^{x^2}(L)$ to behave as follows

$$m^{x^2}(L) = m^{x^2}(\infty) + \frac{\mu}{L^{\frac{1+R}{2}}} \quad (4.7)$$

or as follows

$$m^{x^2}(L) = m^{x^2}(\infty) + \frac{\mu_{\frac{1}{2}}}{\sqrt{L}} + \frac{\mu_1}{L} + \dots \quad (4.8)$$

The $\frac{1}{\sqrt{L}}$ scaling which appears in (4.7) and (4.8) as $R \rightarrow 0$ (as well as in (4.6) for $R = 0$) when applied to accessible small systems works poorly probably because L is still too small.

To summarize, using the data for $N = 16, 36$ and $N = 8, 18, 32$ clusters and scaling laws (4.3) and (4.5) we find $e_0(\infty)$ and $m^{x^2}(\infty)$ (and the order parameter $m = \sqrt{m^{x^2} + m^{y^2}} = \sqrt{2m^{x^2}}$). We use these findings for the discussion in the next Section. Let us also remark, that the presented discourse refers to the case $\gamma = 0$, whereas the case of anisotropic exchange interaction $\gamma \neq 0$ was not considered.

5 Effects of the spatial and exchange interaction anisotropies

In this Section we discuss the results for the ground-state energy, the order parameter and the specific heat obtained by the different methods illustrated in Sections 2, 3, 4. We also compare the approximate and exact results when available.

In Fig. 1 we show the ground-state energy of the square-lattice $s = \frac{1}{2}$ XY model obtained within various approaches in comparison with some exact results (the 1D limit and the Ising limit). As can be seen from Eq. (3.9), (3.6) the Jordan-Wigner fermions for the XY model (short-dashed curves) recover the 1D limit ($R = 0$, $R = \infty$). In the other limit of the Ising model ($\gamma = 1$) this approach fails (obviously except the 1D limit $R = 0$, $R = \infty$). The Jordan-Wigner fermions for XZ model (long-dashed curves) correctly reproduce the dependence e_0 vs. R for $\gamma = 1$ but not the exact results for $R = 0$. We also show the dependence e_0 vs. $-\gamma$ obtained within the latter approximation (thin long-dashed curves with cusps) to demonstrate explicitly a difference in the outcomes as γ changes its sign. It should be remarked that the linear spin-wave theory predictions for the ground-state energy (2.9) (dotted curves) are in a satisfactory agreement with the exact results for $R = 0$ (except small γ),

coincide with the exact result for $\gamma = 1$ and are in a good agreement with the exact diagonalization data for $\gamma = 0$ (full squares).

The XZ model within the fermionic picture exhibits in-plane magnetization introduced by decoupling (3.13), which is determined self-consistently by Eq. (3.19). Fig. 2 shows the resulting dependence of the ground-state magnetization m^z (long-dashed curves) on γ for $R = 1$ (curves 3), $R = 0.5$ (curves 2), and $R = 0$ (curves 1). The value of m^z for $R = 1$ overestimates the exact diagonalization result at $\gamma = 0$ (full square). Moreover, the magnetization does not disappear in 1D limit at $\gamma = 0$ that contradicts the rigorous statement and indicates the incorrect treatment of strong quantum fluctuations in one dimension. The exact zero-temperature relation between in-plane magnetization and exchange anisotropy parameter in 1D reads $m = \frac{1}{2} \left(1 - \left(\frac{1-\gamma}{1+\gamma} \right)^2 \right)^{\frac{1}{4}}$ [32] (solid curves 1 in Fig. 2). The linear spin-wave theory results (2.10) (dotted curves) are valid only for $\gamma \geq 0$ as was explained in Section 2. (Therefore, within the frames of the linear spin-wave theory we cannot trace the behaviour of m^z (for example, for $R = 1$) when decreasing γ to negative values.) Contrary to the fermionic description the linear spin-wave theory predicts smaller values of m^z at $\gamma = 0$ in a good agreement with the exact diagonalization data (see the upper inset in Fig. 2). The linear spin-wave theory value of m^z for $\gamma = 0$ decreases as R decreases and finally becomes zero at a certain small but nonzero value of R . If $R \rightarrow 0$ the value of m^z for $\gamma = 0$ tends to $-\infty$ which is a manifestation of the inapplicability of the linear spin-wave theory in the 1D limit (see the lower inset in Fig. 2 where the spin-wave theory result for $R = 0$ is shown).

Let us consider the dependence of the ground-state in-plane magnetization on γ as it issues from the fermionic picture in more detail. Assume, for example, the spatially isotropic case $R = 1$. From exact results for this model we know that for $\gamma = 1$ the order parameter $m = \frac{1}{2}$ is directed along z axis, whereas for $\gamma = +0$ the order parameter is $0 < m < \frac{1}{2}$ and it remains directed along z axis. If γ becomes negative (tending to -1) two possibilities are plausible: i) for infinitesimally small $\gamma = -0$ the order parameter m turns to the x axis and its value starts to increase (approaching $\frac{1}{2}$ as $\gamma \rightarrow -1$); ii) the order parameter m remains directed along z axis and its value decreases until a certain characteristic value of (negative) γ at which m abruptly turns to x axis and then its value starts to increase (approaching $\frac{1}{2}$ as $\gamma \rightarrow -1$). The fermionization approach results give evidence in favour of the latter scenario. To illustrate this issue we show in Fig. 3 the ground-state energy (given by (3.18) as $\beta \rightarrow \infty$) for spatially isotropic ($R = 1$) XZ model as a function of m^z or m^x (see the comments after Eq. (3.13)) for several values of $\gamma < 0$. The profiles plotted in the left panel exhibit one minimum at $m^z \neq 0$ for $\gamma_1 < \gamma < 0$ (curve 1), two minima at $m^z \neq 0$ (the deeper one) and at $m^z = 0$ for $\gamma_2 < \gamma < \gamma_1$ (curve 2), two minima at $m^z \neq 0$ and at $m^z = 0$ of the same depth for $\gamma = \gamma_2$ (curve 3), two minima at $m^z \neq 0$ and at $m^z = 0$ (the deeper one) for $\gamma_3 < \gamma < \gamma_2$

(curve 4), and one minimum at $m^z = 0$ for $\gamma_3 < \gamma$. (The curve m^z vs. γ in Fig. 2 jumps to zero value at $\gamma = \gamma_3$.) The profiles plotted in the right panel represent the dependence of the ground-state energy for the same γ s on the order parameter directed along x axis. From these plots we see that for $\gamma < 0$ the minimum in the dependence e_0 vs. m^x is always deeper than the one in the dependence e_0 vs. m^z and hence the x directed order parameter is favourable. However, while decreasing γ from positive values to negative ones the system may remain in the metastable phase with the order parameter directed along z axis until γ achieves γ_3 . This is a typical scenario of the first-order quantum phase transition driven by the exchange interaction anisotropy γ . The corresponding region of metastability in the $\gamma - R$ -plane is shown in Fig. 4. The obtained issue can be compared with the predictions of other approaches. The linear spin-wave theory does not work if $\gamma < 0$ and thus cannot be used for this discussion. The coupled cluster method and the correlated basis function method similarly to the 2D Jordan-Wigner fermionization approach suggest an analogous behaviour of the ground-state energy [24, 25]. Moreover, the correlated basis function prediction for the value of $\gamma = -0.36$ associated with a phase transition for spatially isotropic square-lattice [25] is quite close to the estimate obtained by the fermionization approach $\gamma_3 = -0.3528$. An intriguing question naturally arises here: is the described scenario of a first-order quantum phase transition inherent in the spin model or it is an artifact of the approximate approaches? This question, apparently, cannot be answered by the mentioned theories and more work is necessary to draw a definite conclusion.

Next we pass to another interesting problem, that is, the appearance/disappearance of the long-range order at zero temperature in quasi-1D limit. It is known that there is no long-range order for the 1D ($R = 0$) isotropic ($\gamma = 0$) XY model and it does exist for the spatially isotropic 2D ($R = 1$) isotropic ($\gamma = 0$) XY model. If $\gamma = 1$ the order parameter takes its classical value $m = \frac{1}{2}$ for all $0 \leq R \leq 1$. Let us consider the dependence m vs. R which arises within different approaches. The prediction for the order parameter m^z vs. R as it follows from the Jordan-Wigner picture for the XZ model with $\gamma = 0$ is shown in Fig. 5 by long-dashed curve. The exact result $m^z = 0$ for $R = 0$ is not reproduced. The result of the linear spin-wave theory is shown in Fig. 5 by dotted curve. The linear spin-wave theory does not work properly as $R \rightarrow 0$ yielding $m^z \rightarrow -\infty$. To make this explicit, we insert (2.7) into (2.10) and note that the integrand diverges at $R = 0$, $\gamma = 0$ around $k_x = 0$. We expand the integrand about small k_x to pick up the main contribution to the integral in the limit $R, \gamma \rightarrow 0$. For $\gamma = 0$, $R \rightarrow 0$ we get

$$m^z = \frac{1}{4\sqrt{2\pi}} \ln R + \text{finite terms.} \quad (5.1)$$

For finite $\gamma > 0$ the order parameter m^z is finite for all $0 \leq R \leq 1$; if $R = 0$ the order parameter again has a logarithmic divergence as $\gamma \rightarrow 0$, $m^z = \frac{1}{4\sqrt{2\pi}} \ln \gamma + \text{finite terms}$; for finite $R > 0$ the order parameter m^z is finite

for all $0 \leq \gamma \leq 1$. The dotted curve in Fig. 5 for very small R reproduces the logarithmic divergence for $\gamma = 0$ and the characteristic value of R at which m^z becomes zero is about $7 \cdot 10^{-4}$. We also report the exact diagonalization data for the $N = 36$ lattice shown by empty squares in the main plot in Fig. 5 as well as the finite-size scaling (4.5) predictions from square and diamond shaped clusters shown by full squares and full diamonds, respectively. According to (4.5) $m^x(\infty)^2$ becomes negative for R in between 0.03 and 0.04 (diamond shaped clusters) or in between 0.04 and 0.05 (square shaped clusters) (see, for example, two lower curves in the inset in Fig. 5 which refer to the square shaped clusters) that we may take as a criterion for disappearance of the long-range order as the spin system is becoming a collection of noninteracting chains.

We may summarize our findings as follows: for the spatially anisotropic 2D $s = \frac{1}{2}$ isotropic (i.e., $\gamma = 0$) XY (XZ) model the 2D Jordan–Wigner fermionization approach predicts long-range order for any $0 \leq R \leq 1$, the linear spin-wave theory for $R > R_c$ with R_c about $7 \cdot 10^{-4}$, the finite-size scaling data (4.5) for $R > R_c$ with R_c in between 0.03 and 0.05. It should be remarked that the results of the performed analysis are qualitatively similar to what have been obtained for weakly coupled $s = \frac{1}{2}$ isotropic Heisenberg chains [10, 11, 12] (see also a recent study for a 2D array of interacting two-leg $s = \frac{1}{2}$ Heisenberg ladders [13]). Note, however, that the exact diagonalization data prediction for R_c for the XY Hamiltonian is in between 0.03 and 0.05 whereas for the Heisenberg Hamiltonian R_c is essentially larger been in between 0.2 and 0.3 (see Fig. 2 of Ref. [12]). For both systems, i.e., the isotropic XY model and the isotropic Heisenberg model the question about developing of the long-range order as the interchain interaction starts to increase is far from being settled and more delicate approaches are necessary to resolve this question.

Let us turn to the properties of the considered square-lattice $s = \frac{1}{2}$ model at nonzero temperatures. In Fig. 6 we show the temperature dependence of the specific heat for the XY model (3.11) (short-dashed curves) and XZ model (which follows from (3.18), (3.19)) (long-dashed curves) in comparison with the exact results (solid curves) for $R = 0$ and the Onsager solutions (for $\gamma = 1$) [33] as well as with the quantum Monte Carlo result for $\gamma = 0$, $R = 1$ [19] (open squares). Eq. (3.11) yields exact result in 1D limit. The noninteracting Jordan–Wigner fermions (3.7), (3.6) cannot reproduce the logarithmic singularity inherent in the spin model for $\gamma = 1$ (however, recover the exact result as the square-lattice Ising model becomes a set of noninteracting Ising chains). The temperature dependence of the specific heat for XZ model as it follows from (3.18), (3.19) has a mean-field character exhibiting an incorrect finite jump. A noticeable difference between the outcomes of the quantum Monte Carlo and 2D Jordan–Wigner fermionization approaches for $\gamma = 0$, $R = 1$ is seen at low and intermediate temperatures. Recently the temperature dependence of the specific heat for $\gamma = 0$, $R = 1$ has been examined within the Green’s-function approach [26].

The obtained temperature profile (Fig. 2 of that paper) although is in qualitative agreement with the quantum Monte Carlo data but exhibits a lower peak at a higher temperature.

In Fig. 7 we plot the temperature dependence of the in-plane magnetization for spatially isotropic 2D ($R = 1$) XZ model derived within the 2D Jordan–Wigner fermionization scheme (long-dashed curves) and the exact result for $\gamma = 1$ (solid curve). For $R = 1$, $\gamma = 1$ the approximate result based on the fermionization approach (long-dashed curve 3 in Fig. 7) is the mean-field counterpart of the Onsager solution (solid curve 3 in Fig. 7). The approximate result for $R = 1$, $\gamma = 0$ (long-dashed curve 1 in Fig. 7) is incorrect since the Mermin–Wagner theorem predicts $m = 0$ at any finite temperature for the isotropic XY model. For $R = 0$ the fermionization approach yields decreasing of m^z as temperature increases and vanishing of m^z at a certain temperature instead of the correct behaviour $m = 0$ for any finite temperature.

6 Summary

To summarize, we have extended the 2D Jordan–Wigner fermionization approach for the *anisotropic* square-lattice $s = \frac{1}{2}$ XY model. In our study of the ground-state properties we have concentrated on the effects of i) exchange interaction anisotropy and ii) spatial anisotropy. We have analyzed 1) the quantum phase transition driven by the exchange interaction anisotropy and 2) appearance/disappearance of the long-range order in quasi-1D limit. We have discussed these issues using different approaches: 2D Jordan–Wigner fermionization, linear spin-wave theory and exact diagonalization data supplemented by finite-size scaling. The study of the anisotropy driven changes extends the the earlier papers [24, 25] suggesting the first-order quantum phase transition scenario. The study of the 2D-to-1D crossover constitutes the XY counterpart of the problem intensively discussed within the context of the Heisenberg model ([12] and references therein). In our study of the temperature effects we have discussed to what extent the Jordan–Wigner fermions can reproduce the peculiarities of the specific heat for the square-lattice Ising and isotropic XY models as well as the relation to the Mermin–Wagner theorem.

We have found that the 2D Jordan–Wigner fermionization for the XY Hamiltonian works well in quasi-1D limit (especially as $\gamma \rightarrow 0$) for calculating both the ground-state and thermodynamic quantities. Being applied to the XZ Hamiltonian the 2D Jordan–Wigner fermionization gives the ground-state results similar to the linear spin-wave theory. Although both approaches reproduce the existing long-range order in two dimensions (and therefore work well as $\gamma \rightarrow 1$), they overestimate its effects and fail as $R \rightarrow 0$. The temperature effects for the XZ model are poorly reproduced within the 2D Jordan–Wigner fermionization scheme.

Acknowledgments

The present study was partly supported by the DFG (projects 436 UKR 17/7/01 and 436 UKR 17/1/02). O. D. acknowledges the kind hospitality of the Magdeburg University in the summer of 2001 and in the summer of 2002. O. D. thanks the STCU for the support (project #1673). The paper was partly presented at the XII School of Modern Physics on Phase Transitions and Critical Phenomena (Łądek Zdrój, 21 – 24 June 2001) and the 11–th Czech and Slovak Conference on Magnetism (Košice, 20 – 23 August 2001). O. D. thanks the organizers of both meetings and T. V. thanks the organizers of the latter meeting for the support for participation.

References

- [1] E. Manousakis, *Rev. Mod. Phys.* **63**, 1 (1991).
- [2] M. A. Kastner, R. J. Birgeneau, G. Shirane, and Y. Endoh, *Rev. Mod. Phys.* **70**, 897 (1998).
- [3] E. Fradkin, *Phys. Rev. Lett.* **63**, 322 (1989);
A. Lopez, A. G. Rojo, and E. Fradkin, *Phys. Rev. B* **49**, 15139 (1994);
E. Fradkin, *Field Theories of Condensed Matter Systems* (Addison–Wesley Publishing Company: Redwood City, California Menlo Park, California Reading, Massachusetts New York Don Mills, Ontario Workingham, United Kingdom Amsterdam Bonn Sydney Singapore Tokyo Madrid San Juan, 1991), Chapter 7.
- [4] Y. R. Wang, *Phys. Rev. B* **43**, 3786 (1991);
Y. R. Wang, *Phys. Rev. B* **43**, 13774 (1991);
Y. R. Wang, *Phys. Rev.* **46**, 151 (1992).
- [5] M. Azzouz, *Phys. Rev. B* **48**, 6136 (1993);
M. Azzouz, L. Chen, and S. Moukouri, *Phys. Rev. B* **50**, 6233 (1994);
M. Azzouz and C. Bourbonnais, *Phys. Rev. B* **53**, 5090 (1996);
M. Azzouz, B. Dumoulin, and A. Benyoussef, *Phys. Rev. B* **55**, R11957 (1997);
B. Bock and M. Azzouz, *Phys. Rev. B* **64**, 054410-1 (2001).
- [6] Wang Shaofeng, *Phys. Rev. E* **51**, 1004 (1995);
M. S. Kochmański, *Journal of Technical Physics (Warsaw)* **36**, 485 (1995);

- M. S. Kochmański, Phys. Rev. E **56**, 3831 (1997);
 C. D. Batista and G. Ortiz, Phys. Rev. Lett. **86**, 1082 (2001).
- [7] Y. Ji, J. Qi, J. – X. Li, and C. – D. Gong, J. Phys.: Condens. Matter **9**, 2259 (1997);
 X. – J. Fan and C. – D. Gong, Eur. Phys. J. B **7**, 233 (1999);
 Qingshan Yuan, Yumei Zhang, and Hong Chen, Phys. Rev. B **64**, 012414-1 (2001).
- [8] O. Derzhko, Journal of Physical Studies (L’viv) **5**, 49 (2001).
- [9] G. Misguich, Th. Jolicoeur, and S. M. Girvin, Phys. Rev. Lett. **87**, 097203-1 (2001);
 Th. Jolicoeur, G. Misguich, and S. M. Girvin, cond-mat/0204161;
 Ming–Che Chang, and Min–Fong Yang, cond-mat/0204569.
- [10] I. Affleck, M. P. Gelfand, and R. R. P. Singh, J. Phys. A **27**, 7313 (1994).
- [11] T. Miyazaki, D. Yoshioka, and M. Ogata, Phys. Rev. B **51**, 2966 (1995).
- [12] D. Ihle, C. Schindelin, A. Weiße, and H. Fehske, Phys. Rev. B **60**, 9240 (1999).
- [13] L. Capriotti and F. Becca, Phys. Rev. B **65**, 092406-1 (2002).
- [14] O. Derzhko and T. Krokhmal’skii, Acta Physica Polonica B **32**, 3421 (2001);
 O. Derzhko and T. Krokhmal’skii, J. Magn. Magn. Mater. **242–245**, 778 (2002).
- [15] D. D. Betts, $X – Y$ Model. In: Phase Transitions and Critical Phenomena, Volume 3 Series Expansions for Lattice Models. Edited by C. Domb and M. S. Green (Academic Press, London, 1974), p. 569 – 652.
- [16] E. Loh, Jr., D. J. Scalapino, and P. M. Grant, Phys. Rev. B **31**, 4712 (1985).
- [17] G. Gomez–Santos and J. D. Joannopoulos, Phys. Rev. B **36**, 8707 (1987).
- [18] T. Kennedy, E. H. Lieb, and B. S. Shastry, Phys. Rev. Lett. **61**, 2582 (1988).
- [19] H. – Q. Ding, Phys. Rev. B **45**, 230 (1992).
- [20] Shiwei Zhang and K. J. Runge, Phys. Rev. B **45**, 1052 (1992).
- [21] C. J. Hamer, T. Hövelborn, and M. Bachhuber, J. Phys. A **32**, 51 (1999).
- [22] A. W. Sandvik and C. J. Hamer, Phys. Rev. B **60**, 6588 (1999).

- [23] C. J. Hamer, J. Oitmaa, Zheng Weihong, Phys. Rev. B **43**, 10789 (1991);
Zheng Weihong, J. Oitmaa, and C. J. Hamer, Phys. Rev. B **44**, 11869 (1991).
- [24] D. J. J. Farnell, S. E. Krüger, and J. B. Parkinson, J. Phys.: Condens. Matter **9**, 7601 (1997).
- [25] D. J. J. Farnell and M. L. Ristig, cond-mat/0105386.
- [26] C. Schindelin, H. Fehske, H. Büttner, and D. Ihle, J. Magn. Magn. Mater. **226–230**, 403 (2001).
- [27] O. Derzhko, J. Richter, and T. Verkholyak, Acta Physica Polonica B **32**, 3427 (2001);
O. Derzhko, J. Richter, and T. Verkholyak, Czechoslovak Journal of Physics **52**, A41 (2002).
- [28] D. C. Mattis, The Theory of Magnetism I. Statics and Dynamics (Springer–Verlag: Berlin Heidelberg New York, 1981), Chapter 5.
- [29] P. Hasenfratz and F. Niedermayer, Z. Phys. B **92**, 91 (1993).
- [30] C. J. Hamer, J. Phys. A **19**, 3335 (1986).
- [31] Y. Nonomura, J. Magn. Magn. Mater. **140–144**, 1495 (1995).
- [32] B. M. McCoy, Phys. Rev. **173**, 531 (1968);
E. Barouch and B. M. McCoy, Phys. Rev. A **3**, 786 (1971).
- [33] D. C. Mattis, The Theory of Magnetism II. Thermodynamics and Statistical Mechanics (Springer–Verlag: Berlin Heidelberg New York Tokyo, 1985).

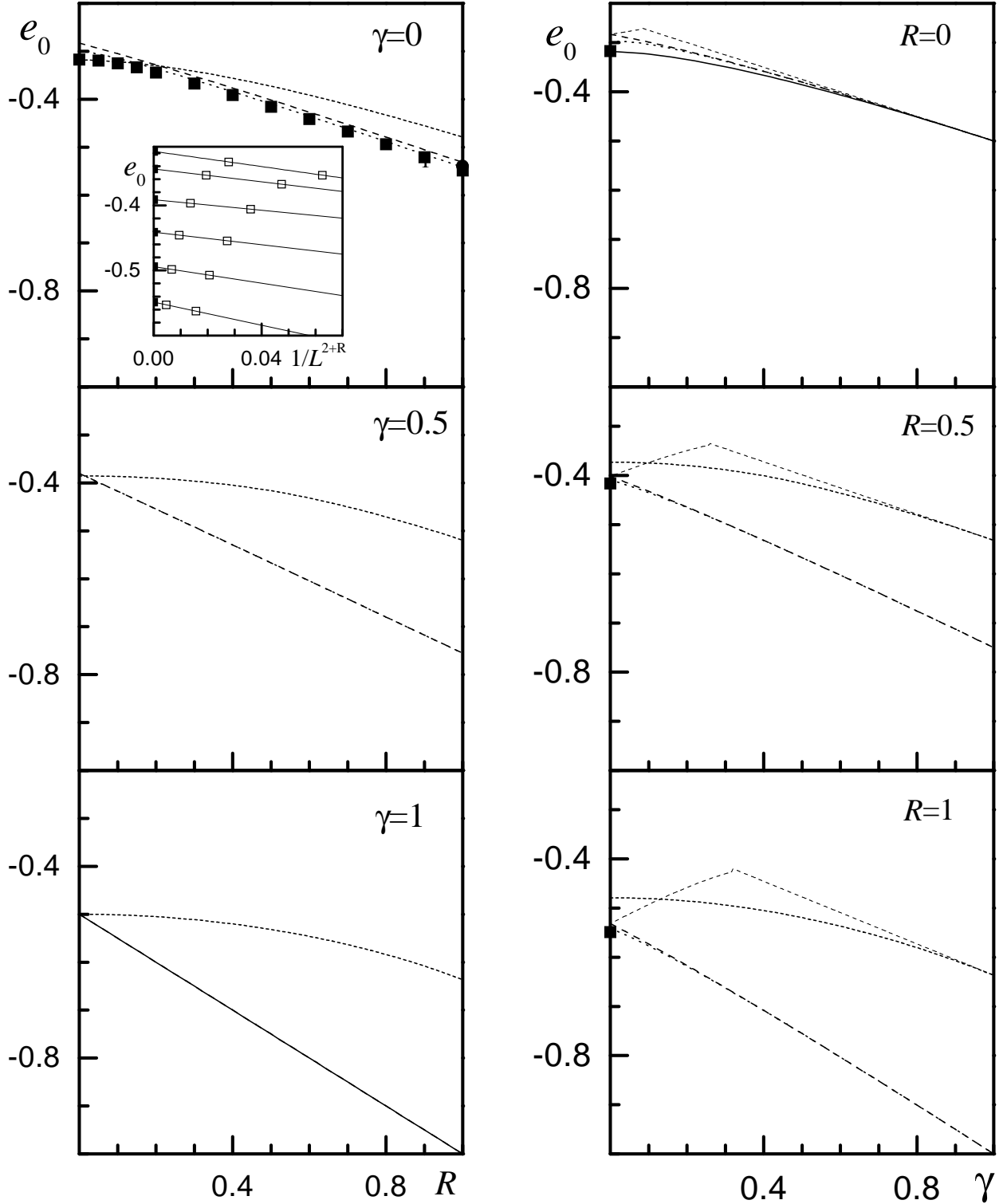


Figure 1: The ground-state energy of the square-lattice $s = \frac{1}{2}$ XY (XZ) model: exact results (solid curves), finite-size extrapolation ($N = 16, 36$) (full squares), linear spin-wave theory (dotted curves), fermionization approach for XY model (short-dashed curves) and XZ model (long-dashed curves). Thin long-dashed curves with cusps in the right panels correspond to the dependence e_0 vs. $-\gamma$ as it follows from (3.18), (3.19) in the limit $\beta \rightarrow \infty$. The inset demonstrates size scaling (4.3) of the finite lattice data ($N = 16, 36$) for $R = 0.8, 0.6, 0.4, 0.2, 0$ (from bottom to top).

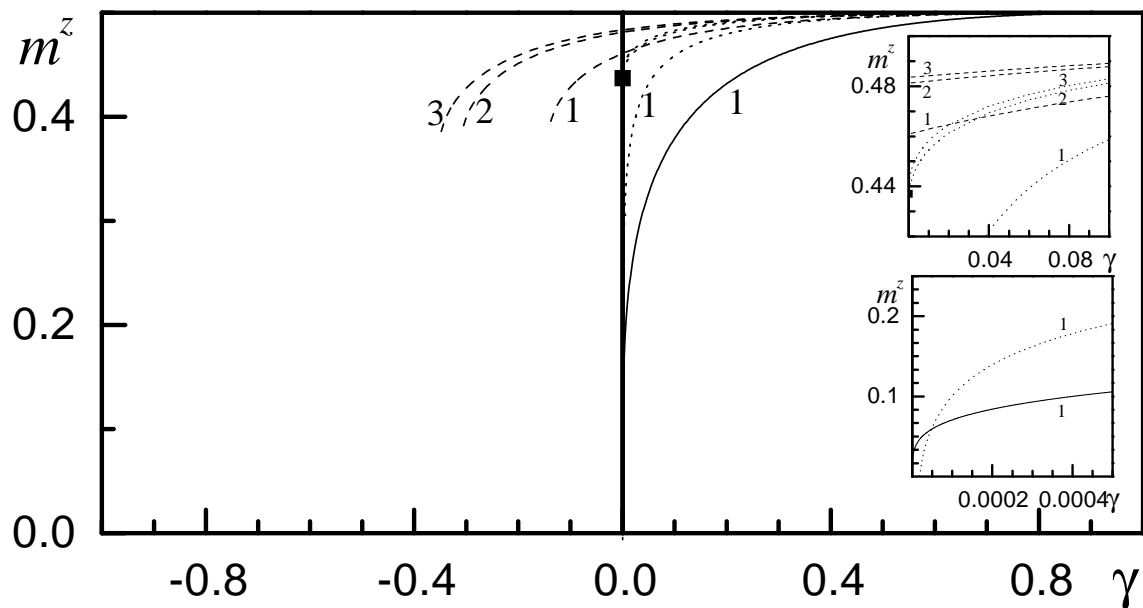


Figure 2: The zero-temperature magnetization m^z vs. the exchange interaction anisotropy parameter γ for square-lattice $s = \frac{1}{2}$ XZ model (1: $R = 0$, 2: $R = 0.5$, 3: $R = 1$): exact result for $R = 0$ (solid curves), finite-size extrapolation result ($N = 16, 36$) for $R = 1$ (full square), linear spin-wave theory results (dotted curves) and fermionization approach results (long-dashed curves). In the lower inset the spin-wave theory result for $R = 0$ becomes negative for γ less than $1.7 \cdot 10^{-5}$.

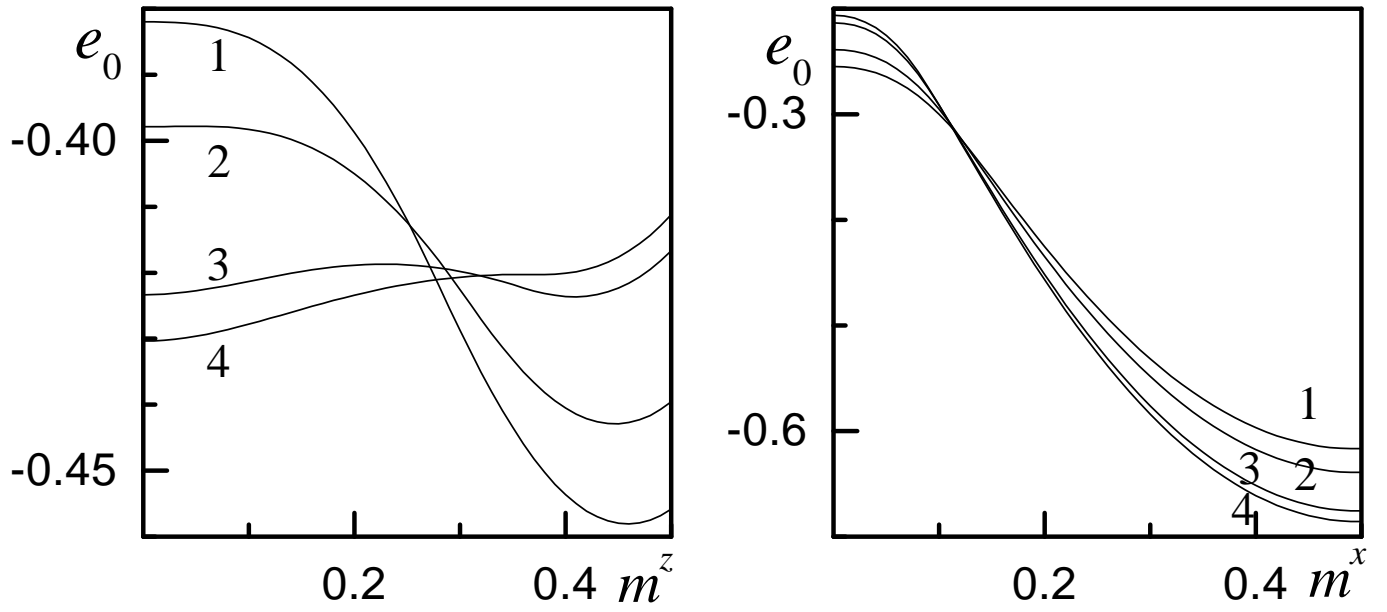


Figure 3: The dependence of the ground-state energy of spatially isotropic ($R = 1$) $s = \frac{1}{2}$ XZ model on the order parameter directed along z (left panel) or x (right panel) axis (obtained from (3.18) as $\beta \rightarrow \infty$) (1: $\gamma = -0.2$, 2: $\gamma = -0.25$, 3: $\gamma = -0.33$, 4: $\gamma = -0.352$).

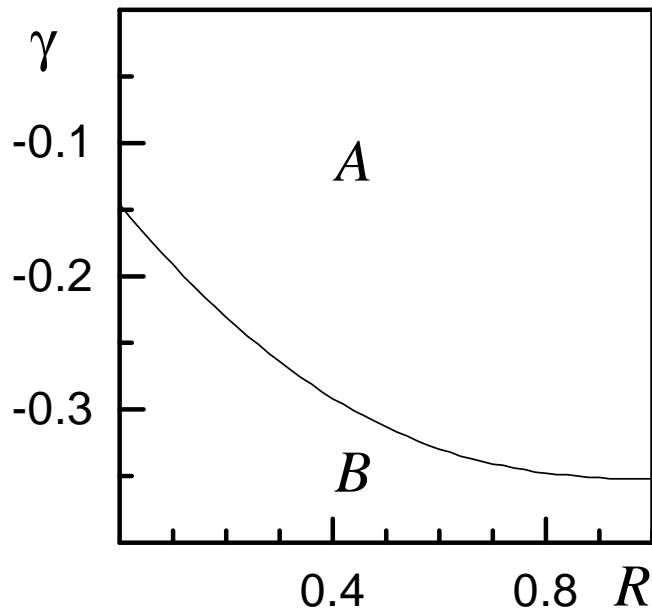


Figure 4: Region of metastability for the square-lattice $s = \frac{1}{2}$ XZ model as it follows from the fermionization approach. For all $\gamma < 0$ the stable phase has $m^z = 0$, $m^x \neq 0$. In the region A the phase with $m^z \neq 0$ is still possible although not favourable (metastable phase), in region B the phase with $m^z \neq 0$ can not exist. The solid curve which separates the regions A and B represents the dependence γ_3 vs. R (see explanation in the main text).

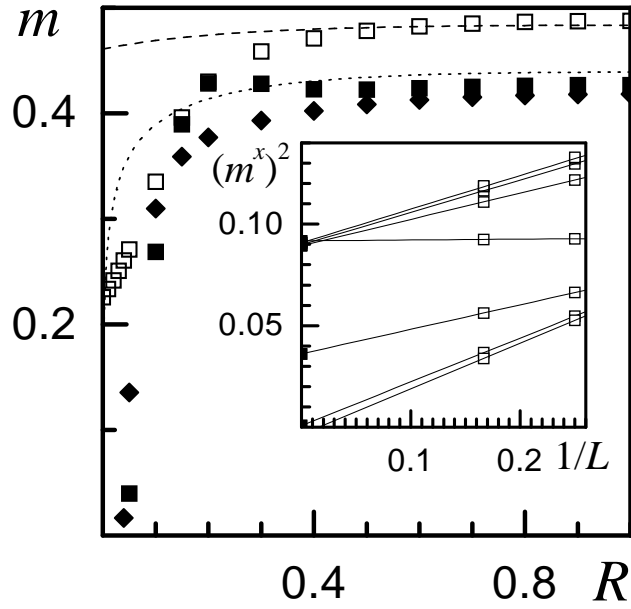


Figure 5: The order parameter for the square-lattice $s = \frac{1}{2}$ isotropic (i.e., $\gamma = 0$) XY (XZ) model as the spatial anisotropy parameter R varies from 0 to 1: exact diagonalization data for $N = 36$ square shaped clusters (empty squares in the main plot), exact diagonalization data completed by scaling (4.5) (square shaped clusters: full squares, diamond shaped clusters: full diamonds), linear spin-wave theory (dotted curve), fermionization approach (long-dashed curve). The linear spin-wave theory result for m becomes zero at R about $7 \cdot 10^{-4}$. The inset demonstrates the size scaling (4.5) of square shaped clusters for $R = 0.04, 0.05, 0.1, 0.2, 0.4, 0.6, 0.8, 1$ (from bottom to top; the curves for $R = 0.8$ and $R = 1$ coincide in the chosen scale).

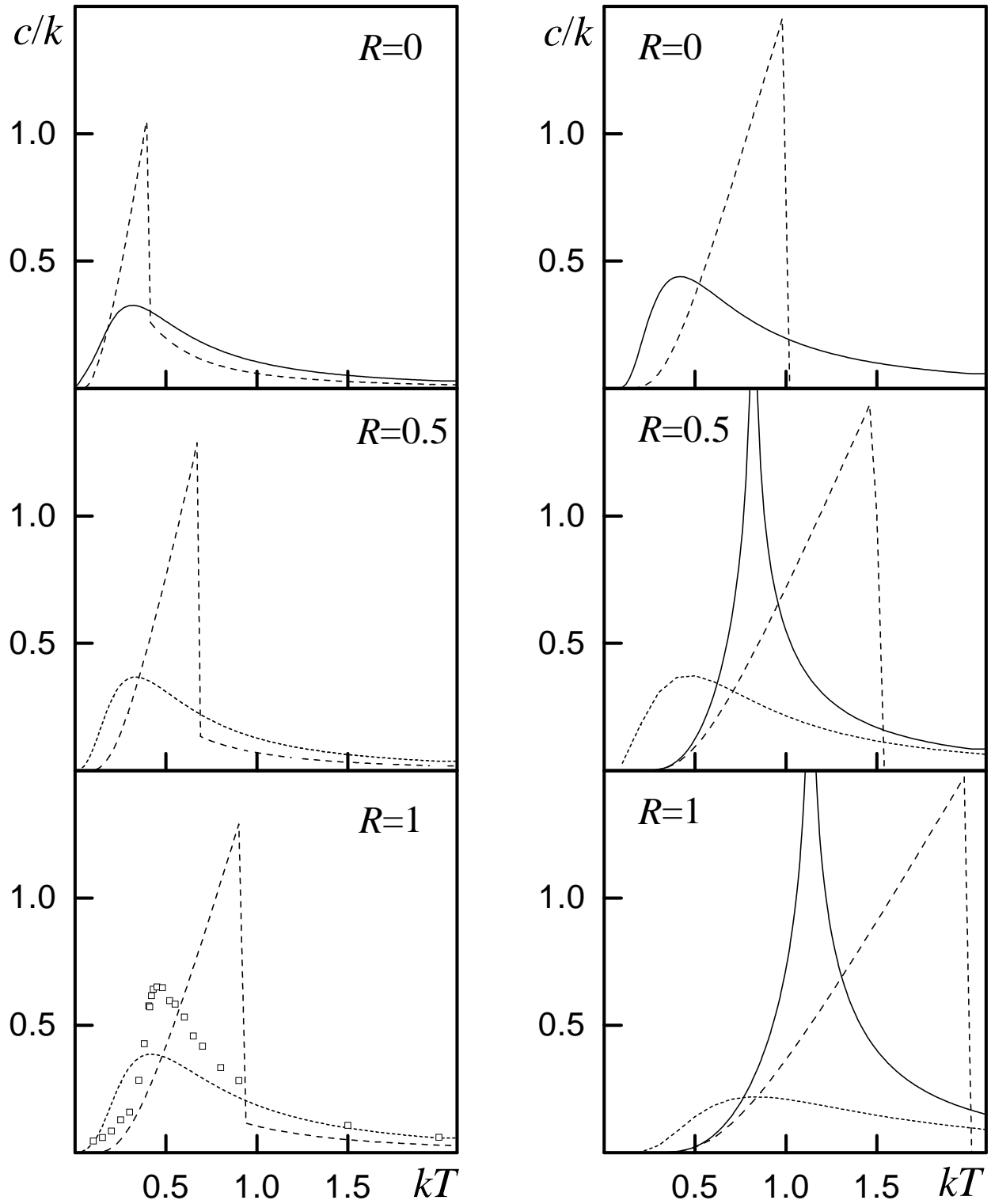


Figure 6: The temperature dependence of the specific heat for the square-lattice $s = \frac{1}{2}$ XY (XZ) model: exact results (solid curves), quantum Monte Carlo result (open squares) [19], fermionization approach results for XY model (short-dashed curves) and for XZ model (long-dashed curves). The left panels refer to the case $\gamma = 0$, the right panels refer to the case $\gamma = 1$. For $R = 0$ (two upper panels) the solid and short-dashed curves coincide.

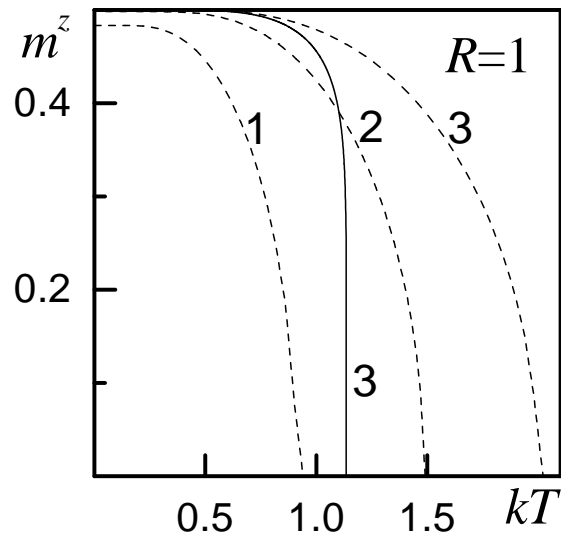


Figure 7: The temperature dependence of the order parameter m^z for spatially isotropic ($R = 1$) $s = \frac{1}{2}$ XZ model (1: $\gamma = 0$, 2: $\gamma = 0.5$, 3: $\gamma = 1$): exact (solid curve) and fermionization approach (long-dashed curves) results.